Carbohydrate Polymers 90 (2012) 1288–1298

Contents lists available at SciVerse ScienceDirect

Carbohydrate Polymers

journal homepage: www.elsevier.com/locate/carbpol

Triamcinolone solubilization by (2-hydroxypropyl)-β-cyclodextrin: A spectroscopic and computational approach

Agnese Miro[a], Francesca Ungaro[a], Federica Balzano[b], Sofia Masi[b], Pellegrino Musto[c], Pietro La Manna[c], Gloria Uccello-Barretta[b,*], Fabiana Quaglia[a,**]

[a] Department of Pharmaceutical and Toxicological Chemistry, University of Naples Federico II, Via D. Montesano 49, 80131, Naples, Italy
[b] Department of Chemistry and Industrial Chemistry, University of Pisa, via Risorgimento 35, 56126 Pisa, Italy
[c] Institute of Chemistry and Technology of Polymers, National Research Council of Italy, via Campi Flegrei, 34, Olivetti Buildings, 80078, Pozzuoli, Naples, Italy

ARTICLE INFO

Article history:
Received 23 January 2012
Received in revised form 11 June 2012
Accepted 25 June 2012
Available online 1 July 2012

Keywords:
Cyclodextrin
Triamcinolone acetonide
Solubility diagram
NMR
Raman
Diffusion

ABSTRACT

The molecular foundations of the use of (2-hydroxypropyl)-β-cyclodextrin (HPβCD) as solubility promoter of triamcinolone acetonide (TrA), a corticosteroid with very low aqueous solubility, was investigated by a multidisciplinary spectroscopic and computational approach. Aqueous solutions of TrA and HPβCD were investigated by UV and NMR spectroscopies. The association constant was determined by phase solubility diagrams and by the Foster–Fyfe method whereas the nature of the drug/cyclodextrin aggregates was probed by using the NMR DOSY technique. ROE measurements in solution led to stereochemical information regarding the nature of inclusion processes. TrA/HPβCD powders were prepared and investigated by Raman spectroscopy supported by computational methods. A molecular interaction of the hydroxyacyl chain with cyclodextrin, not identified in solution, was detected. Raman imaging experiments confirmed the attainment of a molecularly homogeneous system when the TrA/HPβCD molar ratio was 1:7 whereas TrA crystallized for mixtures richer in TrA (1:3.5) forming domains with size in the range of 10–15 μm. We demonstrate that the combined use of several spectroscopical techniques with specific responsivities allows a detailed depiction of drug/cyclodextrin interaction useful in the development of novel pharmaceutical formulation.

1. Introduction

The common goal of drug research is the development of active therapeutic agents, which involves strict synergy between several different disciplines. Very composite problems must be faced which receive converging contributions from medicinal chemistry, pharmaceutics, chemistry and physical chemistry. Nowadays, the properties of new chemical entities are shifting towards higher molecular weight and increasing lipophilicity that raises severe limitations of solubility and in turn bioavailability. As a consequence, a great deal of efforts is addressed towards the development of new strategies at the preformulation stage with the aim to develop robust formulations (Waring, 2010). Very subtle structural changes in the drug may be responsible for dramatic variations of the dissolution response in the presence of the selected solubilizing excipients.

Cyclodextrins have a well-recognized role as solubilizing agents: they have a highly preorganized structure endowed of an external hydrophilic surface, which is responsible for their solubility in aqueous medium, and a hydrophobic cavity inside which lipophilic molecules or molecular portions are included and hence driven in the aqueous medium. The solubilizing power of the host depends on several factors, such as the intrinsic aqueous solubility of the cyclodextrin, its structure and the suited fit between the host cavity and the guest sizes, which affect the strength of the drug–cyclodextrin interaction, and, hence, also the ability to release the drug from the complex (Brewster & Loftsson, 2007; Duchêne, 2011; Loftsson & Duchêne, 2007).

In view of the very composite phenomena on which the use of cyclodextrins as solubility promoters rely on, the knowledge of the molecular basis of host–guest complexation processes would be highly beneficial in order to pursue the rational design of new formulation strategies. Characterization of complexes in both solution and solid state is of crucial importance also at regulatory level when a new drug/cyclodextrin product is examined to receive a market authorization. The resolution of this difficult problem is frequently assigned to the refinement of formulation techniques based on the observation of molecular parameters related to the molecular structure as a whole.

* Corresponding author. Tel.: +39 0502219232.
** Corresponding author. Tel.: +39 081678707.
E-mail addresses: gub@dcci.unipi.it (G. Uccello-Barretta), quaglia@unina.it (F. Quaglia).

0144-8617/$ – see front matter © 2012 Elsevier Ltd. All rights reserved.
http://dx.doi.org/10.1016/j.carbpol.2012.06.075

Among spectroscopic methods Nuclear Magnetic Resonance (NMR) represents one of the most powerful techniques as several structure dependent NMR parameters can be observed. They are exploited both to give very accurate models of the drug–cyclodextrin aggregates as well as to perform very fast and accurate quantitative analysis of the solubilization processes. Importantly, the role of supramolecular aggregation that underlies the processes of solubilization can be thoroughly investigated by exploiting the considerable potential of DOSY (Diffusion Ordered SpectroscopY) NMR measurements of the diffusion coefficients. Spectroscopic and computational methods have great potential in this field due to the fact that several aspects of the molecular recognition processes involved in the drug–cyclodextrin interaction can be efficiently ascertained: association constants and complexation stoichiometry and, importantly, the stereochemical and dynamics features of the drug–cyclodextrin supramolecular aggregates can be investigated.

Raman spectroscopy is an emerging technique that has been successfully applied for studying the formation of inclusion compounds (Smith & Dent, 2005). Advantages of this approach arise from the high spectroscopic contrast, the spectrum resolution, the sensitivity of the technique (provided that spurious effects – like fluorescence – do not interfere) and the wealth of molecular information contained in the vibrational spectrum. Raman investigations have been predominantly carried out in the solid state, taking advantage of the sampling capabilities of the technique, especially when confocal microspectroscopy measurements are involved (Hendra, 2006; Keresztury, 2002; Shrader, 2002). In this respect, Raman studies represent an ideal complement to NMR and UV spectroscopies, both concerned mainly with measurements in solution state.

Spectroscopic methods relying on the observation of different nuclei or functional groups constituting the system under consideration could lead to a deeper understanding of the processes of solubilization and, especially, real molecular models of the drug–excipient supramolecular aggregates can be constructed on the basis of which solubilization process can be rationalized and, hence, optimized.

Triamcinolone acetonide (TrA) (Fig. 1) is a lipophilic synthetic corticosteroid sparely water soluble, which is used to treat various skin conditions and to relieve the discomfort of buccal aphtae. To develop effective drug delivery systems for TrA, strategies to enhance its aqueous solubility are of great importance as well as understanding how this occurs on the basis of mode of interaction with a hydrotropic agent. At the same time, achievement of solid TrA in a fast dissolving solid is critical for dosage forms where drug release is activated by drug solubilization in aqueous media.

In the present contribution we addressed our efforts towards a more comprehensive approach to the solubilization processes of TrA by hydroxypropyl-β-cyclodextrin (HPβCD, Fig. 1) and to the preparation of solid TrA/HPβCD binary systems with improved dissolution properties. For the quantitative analysis of the solubilization processes we used both UV and NMR methods, whereas stereochemical features of TrA, HPβCD and their supramolecular aggregates were investigated in solution by using NMR methods of detection of through space dipole–dipole interactions. Solid-state features were investigated by Raman spectroscopy with the help of computation methods.

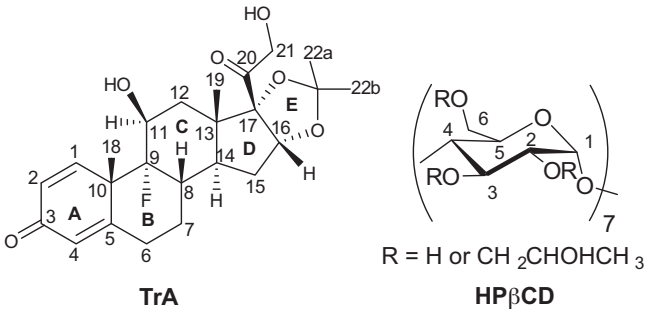

Fig. 1. TrA and HPβCD structures with numbering scheme for NMR analysis.

2. Experimental

2.1. Materials

(2-Hydroxypropyl)-β-cyclodextrin (HPβCD, MS = 0.97, MW = 1529.5 Da), was kindly offered by Roquette Freres (France). Triamcinolone acetonide (TrA, MW 434.5 Da, 99.5% purity) was from Farmalabor (Italy). Potassium phosphate dibasic and potassium phosphate monobasic were from Sigma–Aldrich. Ethanol (96°) was from Carlo Erba (Italy).

2.2. NMR measurements

NMR measurements were performed on a spectrometer operating at 600 MHz for ^{1}H nuclei. The temperature was controlled to ±0.1 °C. The 2D NMR spectra were obtained by using standard sequences with the minimum spectral widths required. Proton 2D gCOSY (gradient COrrelated SpectroscopY) spectra were recorded with 128 increments of 2 scans and 2 K data points. The relaxation delay was 2 s. 2D TOCSY (TOtal Correlation SpectroscopY) spectra were recorded by employing a mixing time of 80 ms. The pulse delay was maintained at 2 s; 256 increments of 4 scans and 2 K data points each were collected. The 2D ROESY (Rotating-frame Overhauser Enhancement SpectroscopY) experiments were performed by employing a mixing time of 0.3 s or 0.6 s. The pulse delay was maintained at 3 s; 256 increments of 6 scans and 2 K data points each were collected. The gradient ^{1}H,^{13}C gHSQC (gradient Heteronuclear Single Quantum Correlation) and gHMBC (gradient Heteronuclear Multiple Bond Coherence) were recorded with 256 or 128 time increments of 16–64 scans. The gradient HMBC experiments were optimized for a long-range ^{1}H—^{13}C coupling constant of 8 Hz and a delay period of 3.5 ms for suppression of one-bond correlation signals. No decoupling was used during the acquisition. DOSY experiments were carried out by using a stimulated echo sequence with self-compensating gradient schemes, a spectral width of 8000 Hz and 64 K data points. A value of 100 ms was used for the diffusion delay, 2.0 ms for the gradient pulse duration, and gradient strength was varied in 15 steps (16 transients each) to obtain an approximately 90–95% decrease in the resonance intensity at the largest gradient amplitude. The baselines of all arrayed spectra were corrected prior to processing the data. After data acquisition, each FID (Free Induction Decay) was apodized with 1.0 Hz line broadening and Fourier transformed. The data were processed with the DOSY macro (involving the determination of the resonance heights of all the signals above a pre-established threshold and the fitting of the decay curve for each resonance to a Gaussian function) to obtain pseudo two dimensional spectra with NMR chemical shifts along one axis and calculated diffusion coefficients along the other.

^{1}H NMR (600 MHz, CD_3OD, 25 °C) parameters for TrA (see Fig. 1 for the numbering scheme): δ 0.90 (3H, Me-19, s), 1.14 (3H, Me-22a, s), 1.39 (3H, Me-22b, s), 1.50 (1H, H_{7ax}, m), 1.58 (3H, Me-18, s), 1.60 (1H, H_{12eq}, m), 1.63 (2H, H_{15}, m), 1.91 (1H, H_{7eq}, m), 2.06 (1H, H_{14}, m), 2.19 (1H, H_{12ax}, dt, J_{12ax-F} = 13.9 Hz, $J_{12ax-12eq}$ = $J_{12ax-11}$ = 3.6 Hz), 2.40 (1H, H_{6eq}, ddd, $J_{6eq-6ax}$ = 13.8 Hz, $J_{6eq-7ax}$ = 5.1 Hz, J_{6eq-4} = 1.8 Hz), 2.54 (1H, H_8, dtd, J_{8-F} = 28.9 Hz, J_{8-14} = J_{8-7ax} = 12.0 Hz, J_{8-7eq} = 5.0 Hz,), 2.72 (1H, H_{6ax}, tdd, $J_{6ax-6eq}$ = $J_{6ax-7ax}$ = 13.8 Hz, $J_{6ax-7eq}$ = 6.1 Hz, J_{6ax-4} = 1.8 Hz),

4.18 (1H, H_{21b}, d, $J_{21b-21a}$ = 19.1 Hz,), 4.27 (1H, H_{11}, ddd, J_{11-F} = 9.6 Hz, $J_{11-12ax}$ = 3.6 Hz, $J_{11-12eq}$ = 2.4 Hz), 4.68 (1H, H_{21a}, d, $J_{21a-21b}$ = 19.1 Hz,), 5.02 (1H, H_{16}, t, J_{16-15} = 2.6 Hz), 6.09 (1H, H_4, t, 1.8 Hz), 6.29 (1H, H_2, dd, J_{2-1} = 10.1 Hz, J_{2-4} = 1.8 Hz), 7.38 (1H, H_1, d, J_{1-2} = 10.1 Hz).

2.3. Raman Spectroscopy

The Raman spectra were collected by a confocal Raman spectrometer (Horiba-Jobin Yvon Mod. Aramis) operating with a diode laser excitation source emitting at 532 nm. The 180° back-scattered radiation was collected by an Olympus metallurgical objective (MPlan 50×, NA = 0.75) with confocal and slit apertures both set to 200 μm. A grating with 1200 grooves/mm was used throughout. The radiation was focused onto a Peltier-cooled CCD detector (Synapse Mod. 354308) operating in the Raman-shift range 3200–100 cm^{-1} for single point measurements or in the range 1800–100 cm^{-1} in the case of the mapping experiments, to reduce the acquisition time.

The data gathered by the instrument were converted into ASCII format and transferred to the MATLAB computational platform for further processing. The Raman images were elaborated by in-house written programs, making use of the image processing facilities and surface interpolating algorithms of the MATLAB environment.

To separate the individual peaks in the case of unresolved, multicomponent profiles, a least-squares curve fitting (LSCF) algorithm was employed, based on the Levenberg–Marquardt method (Meier, 2005). In order to reduce the number of adjustable parameters and to insure the uniqueness of the result, the baseline, the band shape and the number of components were fixed. The program was then allowed to calculate, by a non-linear curve-fitting of the data, the height, the full width at half height (FWHH) and the position of the individual components. The Voigt function (Meier, 2005) was used throughout to simulate the experimental line-shapes.

2.4. Computational details for geometry optimization and normal coordinate analysis

Molecular Mechanics calculations were performed by the Allinger's MM2 force field (Allinger, Kok, & Imam, 1988), as implemented by the Chem3D suite of programs (Chem3D Pro, V11, Cambridgesoft Inc, Massachusetts). Apart from the standard Potential Energy terms (bond stretching, bending, torsion, van der Waals, electrostatic), the MM2 force field also contains stretch-bend cross-terms (Urey–Bradley) which are often critical for accurately simulating complex molecules. Furthermore, the Hydrogen-bonding interactions are taken into account by use of suitably parameterized terms of the van der Waals potential (Allinger et al., 1988). Quantum chemistry calculations were performed using the unrestricted density functional theory (DFT) (Becke, 1993). In particular, the hybrid method referred to as B3LYP was used, in combination with the standard 6-31G(d,p) basis set. This method includes the Becke's three-parameter exchange functional (Becke, 1993) coupled with the Lee–Yang–Parr correlation functional. After the geometry optimization, a normal coordinate analysis at the same level of theory was performed, comprising the calculation of the Hessian matrix (**F**) by analytical evaluation of the first and second derivatives of the potential energy with respect to the Cartesian displacement coordinates. The **F** matrix was then transformed in terms of mass-weighed coordinates and diagonalized to obtain the corresponding eigenvalues (normal frequencies) and eigenvectors (displacement vectors, **L** matrix). Finally, a transformation into a set of redundant internal coordinates of both the **F** and **L** matrices was accomplished in order to characterize the normal modes in terms of their potential energy distribution (PED), expressed, in normalized form, as (Wilson, Decius, & Cross, 1955)

$$(PED)_{jk} = \frac{F_{jj}L_{jk}^2}{\sum_i F_{ii}L_{ik}^2} \cdot 100 \quad (1)$$

where the PED (in %) refers to the contribution of the jth internal coordinate to the kth normal mode, F_{jj} is the jth diagonal Force constant, and L_{jk} is the corresponding element of the **L** matrix. To correct for anharmonicity and for the systematic errors inherent in the calculated frequencies, these were scaled by a factor of 0.9613, as prescribed by Wong, Wiberg, and Frisch, (1991).

In addition to the frequency and atomic displacements of the normal modes, bond polarizabilities were also computed. These allows one to calculate the Raman activities (S_i) which can be converted, according to the general theory of Raman scattering (Keresztury, 2002; Keresztury et al., 1993), to the relative intensities (I_i), making use of the following relationship:

$$I_i = \frac{f(\nu_0 - \nu_i)^4 S_i}{\nu_i(1 - e^{-hc\nu_i/k_bT})} \quad (2)$$

In the above equation ν_0 is the exciting frequency in cm^{-1}, ν_i the wavenumber of the ith normal mode, h, c and k_b are the fundamental constants, T is the absolute temperature and f is a suitably chosen normalization factor for all the peak intensities. All calculations were performed on a HP system model Integrity rx2620, equipped with two parallel Itanium processors. For the DFT and NCA calculations, the program Gaussian 03 (Frisch et al., 2004) was employed. Different graphic interfaces were used (Gaussview, ATOMS) to visualize and represent the normal modes, either in terms of atomic displacements or as animated vibrations, for assignment purposes.

2.5. UV spectrophotometry

TrA quantitative analysis was performed by UV spectrophotometry at the wavelength of 238 nm (UV 1204 spectrophotomer, Shimadzu, Japan). Standards were prepared in ethanol. Linearity of response was verified in the TrA concentration range 1.1–22 μg/mL ($r^2 > 0.998$).

2.6. Solubility measurements

For the phase solubility study, an excess of TrA (50 mg) was added to 25 ml of water containing increasing amounts of HPβCD ranging from 1.0×10^{-3} to 2.8×10^{-1} M (close to maximum water solubility of HPβCD) and shaken in screw-capped glass vials at 25 °C until equilibrium. After 4, 7 and 10 days, an aliquot was withdrawn, filtered (filter HA-0.45 μm, Millipore) and analysed for TrA content by spectrophotometry. Solubility of TrA in water, 50 mM phosphate buffer saline at pH 6.8 (2.38 g Na_2HPO_4, 0.19 g KH_2PO_4, 8 g NaCl per liter adjusted with ortophosphoric acid, referred as PBS in the following), ethanol/water 1/3 v/v solutions, ethanol/water 1/3 v/v solution containing HPβCD was evaluated analogously.

Solubilization experiments by NMR were carried out by suspending the same amount of TrA (5 mg) in different volumes of a stock aqueous solution of the cyclodextrin and by adding D_2O till to the final volume of 1 mL. In this way the maximum concentration of 5.97 mM was reached for the cyclodextrin. The solution was stirred in Vortex for 13 h, then left to decant and the limpid supernatant directly transferred into the NMR tube without filtering. The quantitative NMR analysis of dissolved TrA was performed by using sodium acetate as external standard contained in a coaxial tube.

Assuming the formation of a complex with a 1:1 stoichiometry, the apparent stability constant ($K_{1:1}$) was calculated from the

linear part of the graph obtained by plotting the molar concentration of TrA in the solution *versus* each HPβCD molar concentration according to the equation:

$$K_{1:1} = \frac{\text{slope}}{(1 - \text{slope}) \times \text{intercept}} \quad (3)$$

where *slope*/(1 − slope) is defined as complexation efficacy (CE).

By using the approach developed for the optical spectroscopies and by far extended to NMR measurements, the heteroassociation constant K for the TrA/HPβCD complex was determined also by using the Benesi–Hildebrand equation modified for NMR from Foster and Fyfe (1965). In the measurements, the content of TrA was kept constant at 0.028 mM, while the concentration of HPβCD was ranged from 0 to 5.60 mM. K was derived on the basis of the following equation:

$$\frac{\Delta\delta^A_{obs}}{[B]_t} = K\Delta\delta^A_c - K\Delta\delta^A_{obs} \quad (4)$$

where $\Delta\delta^A_{obs}$ is the difference between the chemical shift of a selected proton of the minor component (A) in the presence of a large excess of the other (B) and in the free state, $[B]_t$ is the total concentration of the species B used in each solution and $\Delta\delta^A_c$ is the difference between the chemical shift of the same resonance of A in the complex and in pure compound.

Each experiment was performed in triplicate; the coefficient of variation associated to each measurement was never greater than 3%.

2.7. Preparation of TrA/CD binary systems

Binary systems were prepared from TrA and HPβCD powders screened through a #170 sieve. Evaporated products (EP) were prepared at TrA/HPβCD mole ratio of 1:7 ($EP_{1:7}$) and 1:3.5 ($EP_{1:3.5}$) by dissolving TrA in ethanol (0.5 or 1 mg/mL for 1:7 and 1:3.5 mol/mol ratio, respectively) and HPβCD in water (4.2 mg/mL). Solutions were mixed at a ethanol/water ratio 1:3 v/v and dried at room temperature in a nylon petri dish.

3. Results and discussion

3.1. Phase solubility study

Effect of cyclodextrins on the solubility of a given species is commonly evaluated through phase solubility diagrams, *i.e.* by measuring the amount of the solubilized species in an aqueous medium as a function of cyclodextrin concentration. Very large host/guest ratios up to cyclodextrin saturation are used and the stability constant is determined based on the initial linear part of the diagram. Usually the solubilized guest amount is evaluated by suitable quantitative techniques. Nuclear Magnetic Resonance (NMR) spectroscopy gives a complementary approach to evaluate with great accuracy the solubilizing effect of cyclodextrin at the lowest host/guest ratios, *i.e.* in the linear region of the solubility diagrams.

Fig. 2A shows the phase solubility diagram of TrA in the presence of different concentrations of HPβCD, as evaluated by UV detection. TrA is neutral and presents an apparent solubility of 0.018 mg/mL. As it can be seen, the amount of dissolved TrA increased along time in the presence of HPβCD up to 0.05 M, whereas it decreased above 0.2 M, resulting in a B_S profile according to Higuchi and Connors (Higuchi & Connors, 1965). From the linear part of the graph, apparent stability constant assuming the formation of a complex with 1:1 stoichiometry was calculated as 1570 M^{-1}.

The same kind of solubility measurements was carried out by detecting the amounts of dissolved TrA in the ^{1}H NMR spectra of the mixtures TrA/HPβCD. Only the first part of the solubility diagram was covered by the NMR data, just in the linear region of the

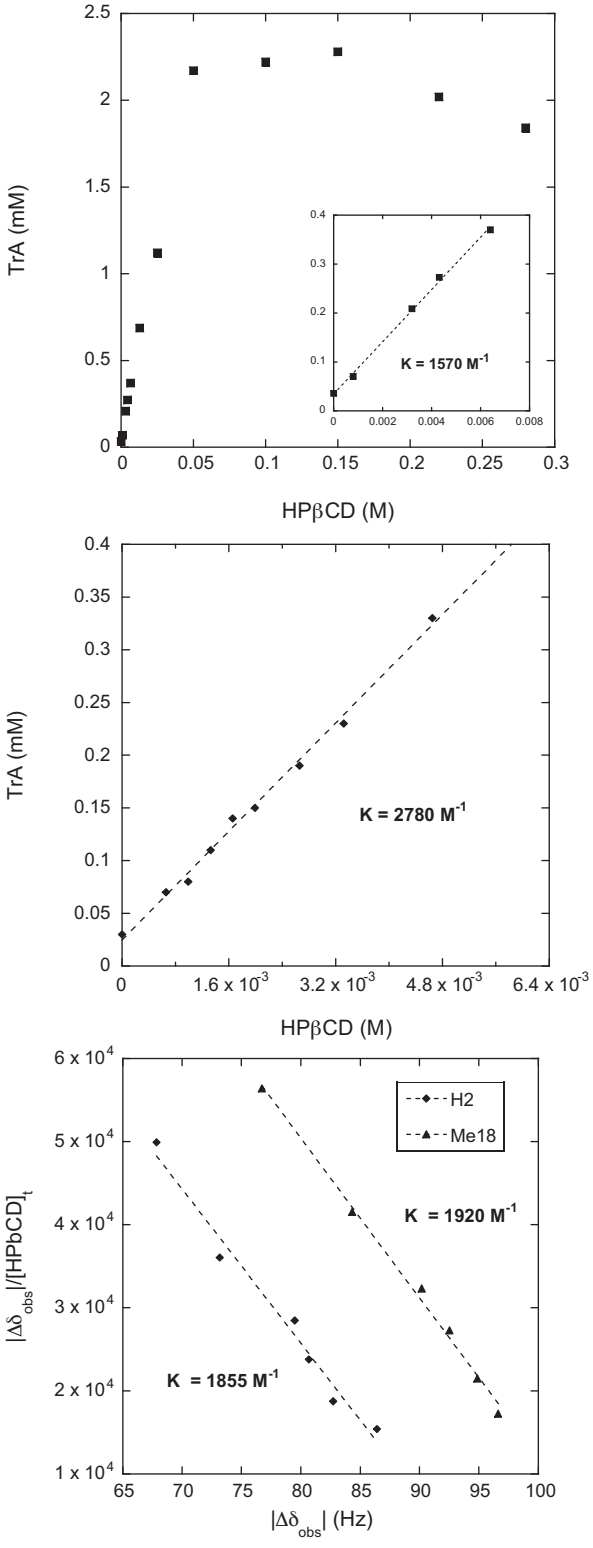

Fig. 2. Solubility of TrA in water solutions containing HPβCD at 25 °C. (A) UV detection Inset: linear part of the phase solubility graph used to calculate stability constant of the complex. (B) NMR solubility in D_2O solutions. (C) NMR determination of the heteroassociation constant of TrA/HPβCD complex in D_2O by the Foster–Fyfe method.

curve (Fig. 2B). The slope of the fitted straight line gave a significantly higher stability constant of 2780 M^{-1}. Above discrepancy is not surprising, taking into account that, mainly for drugs with very low intrinsic solubility (S_0 < 0.1 mg/ml) (Loftsson, Hreinsdottir, & Masson, 2005), $K_{1:1}$ Eq. (3) is critically dependent on S_0, which

should correspond to the intercept of the line. Furthermore, several simultaneously occurring aggregation processes could contribute to the value of the association constant, which make the calculated value strongly dependent also on the method. As reported by Loftsson et al. (Loftsson, Hreinsdottir, & Masson, 2007), the solubilizing efficiency of the cyclodextrins is more reliably described by the complexation efficiency (CE), which gives the ratios between the concentration of the dissolved cyclodextrin complex and the concentration of the dissolved free cyclodextrin. Very similar CE values of 0.056 and 0.069 were respectively obtained by using UV and NMR detection.

Comparison of conventional techniques with an alternative methodology, such as the NMR Foster–Fyfe method, could be greatly advantageous since the method is based on quick and direct measurements of the effect of the complexing agent on any NMR observable parameter (the chemical shift more frequently) and the assumptions regarding the complexation stoichiometry may be efficiently verified also by means of the valuable support of DOSY NMR techniques for the measurement of translational diffusion coefficients.

The Foster–Fyfe method (Foster & Fyfe, 1965) involves different experimental conditions, where the drug is completely solubilized and the effect of the presence of very large excesses of the cyclodextrin is detected by measuring the chemical shifts changes of selected drug protons. In these conditions the occurrence of any possible self-aggregation processes of the drug are strongly discouraged, since the drug is always present in very low concentration and in the presence of a large excess of cyclodextrin.

The change of the chemical shift of the proton H-2 and Me-18 of TrA were measured at 25 °C and the dependence of their $\Delta\delta_{obs}/[HP\beta CD]_t$ on $\Delta\delta_{obs}$ was a straight line (Fig. 2C), the slope of which gave the association constant. The two fittings gave very similar values for the heteroassociation constant, being 1855 M^{-1} ($R = 0.989$) and 1920 M^{-1} ($R = 0.998$) for the olefinic proton H-2 and for the methyl protons Me-18, respectively.

With the purpose to evaluate the reliability of the method, we still have to establish if the complexation phenomena detected by the Foster–Fyfe method may be affected to some extent by any processes of self-aggregation of the cyclodextrin itself or self-aggregation of monomer units of drug–cyclodextrin complexes to give higher order aggregates. In fact, formation of micelle-like supramolecular aggregates of the steroid drug hydrocortisone with HPβCD has been reported (Loftsson, Magnusdottir, Masson, & Sigurjonsdottir, 2002). The parameter that allows to judge on this issue is the translational diffusion coefficient, which is a size dependent parameter and can be measured by using the NMR DOSY (Diffusion Ordered SpectroscopY) technique (Johnson, 1999).

Eq. (5) gives the dependence of the diffusion coefficient on the hydrodynamic radius (R_H) based on the Stokes–Einstein relationship, which strictly holds in the spherical approximation.

$$D = \frac{kT}{6\pi\eta R_H} \tag{5}$$

where k is the Boltzmann constant, T the absolute temperature, and η is the solution viscosity.

Any kind of aggregation phenomenon, which increases the molecular sizes and hence R_H, is expected to bring about a decrease of the diffusion coefficient.

The diffusion coefficient of the cyclodextrin as pure compound was 1.25×10^{-10} m^2 s^{-1} and remained unchanged in the 1:50 and 1:200 TrA/cyclodextrin solutions. The diffusion coefficients (25 °C) were normalized for the small viscosity changes due to the increase of the cyclodextrin concentration by using TMS as internal standard of viscosity (Wimmer, Aachmann, Larsen, & Petersen, 2002). TMS was added in the D_2O solutions (650 μL) dissolved in very small volumes (50 μL) of dimethyl sulphoxide. Thus the occurrence of self-aggregation processes of the cyclodextrin as well as the formation of supramolecular aggregates of complexes can be neglected.

3.2. Stereochemical NMR investigations

3.2.1. Triamcinolone acetonide

TrA (Fig. 1) is rather a rigid molecule, with the rings B and C and the hydroxyacyl fragment at the D–E junction as its unique flexible portions. Direct evidences of the conformational prevalence in solution were obtained by NMR spectroscopy. Due to the scarce solubility of TrA in D_2O we analysed TrA in CD_3OD by which it was solubilized efficiently. The preliminary comparison of ^1H NMR spectra of TrA dissolved in D_2O and CD_3OD (Appendix A, Fig. A.1) demonstrated that the patterns of the spectral parameters in the two solvents were quite similar.

The ^1H NMR spectrum of TrA in CD_3OD was fully assigned by the combined analyses of scalar and dipolar homonuclear and heteronuclear correlation maps 2D TOCSY, COSY, ROESY, HSQC and HMBC. The ^1H NMR spectral parameters are reported in the Section 2.

The conformational investigation was based on the detection by 2D ROESY analyses of the $^1H—^1H$ dipolar interactions through the space, which allowed us to impose constraints of spatial proximity between proton nuclei of TrA. Comparable ROEs $H_1—H_2$ and $H_1—H_{11}$ were detected (Fig. 3a), which imposed the coplanarity of the bonds $C_2—H_2$ and $C_{11}—H_{11}$, in agreement with the equatorial arrangement of the proton H_{11}. The low value (2.4 Hz) of the vicinal coupling constant $^3J_{11-12}$ confirmed the above said conclusion. The expected dipolar interaction between the proton H_1 and the adjacent methyl protons Me-18 was also detected. At the frequency of the proton H_{11} (Fig. 3b) comparable ROEs with the two vicinal protons H_{12} (2.19 ppm, 1.60 ppm) were observed as expected on the basis of its equatorial position. The orientations of the two protons H_{12} were discriminated on the basis of the dipole–dipole interactions they originated. In particular the high-frequency shifted resonance centred at 2.19 ppm was assigned to the axial proton H_{12ax} due the ROE with the proton H_{14} (Fig. 3c) which must lie on the same semiplane.

The proton H_{14} (Fig. 3d) also gave ROE at 1.50 ppm which represents the resonance of one of the two protons H_7 and hence must be axial. It is noteworthy that the relevant high frequencies shifts of the protons H_{14}, H_{12ax} and H_{7ax} can be justified on the basis of their proximity to the fluorine nucleus.

The conformation of the ring named as B was completely defined on the basis of the following effects: the proton H_8 gives significant ROEs at the frequencies of the two methyl groups Me-18 and Me-19 and of the protons H_{6ax} and H_{7eq} (Fig. 3f). Accordingly, the proton H_4 produces ROE almost on the proton H_{6eq} (Fig. 3e). Therefore the ring B mainly assumes a chair conformation with the protons Me-18, H_8 and H_{6ax} in axial position in the same half-plane (Fig. 4).

Strongly differentiated ROEs are produced by the two methyl protons Me-22b (1.39 ppm) and Me-22a (1.14 ppm) which allowed us to identify the high frequency shifted Me-22b methyl as the one bent at H_{12ax} and H_{14}. Similarly strongly differentiated ROEs were detected at the frequencies of the two side chain protons H_{21}, with H_{21a} at 4.68 ppm directed towards the methyl proton Me-22a (Fig. 3g) and H_{21b} at 4.18 ppm bent at H_{12eq} (Fig. 3 h). The very low dipolar interaction with the methyl protons Me-19 suggested a strong conformational prevalence with faced carbonyl and hydroxy groups of the 2-hydroxyacyl chain (Fig. 4), which probably are hydrogen bonded. Some weak unexpected ROEs also suggested the occurrence of self-association phenomena of TrA in solution.

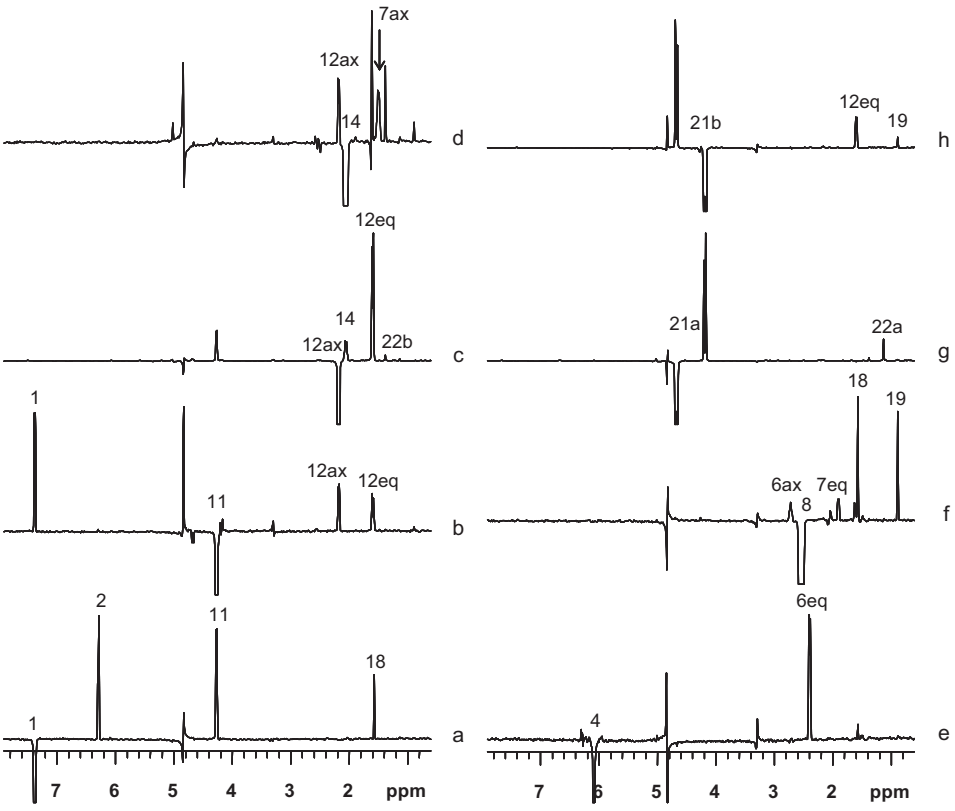

Fig. 3. 2D ROESY (600 MHz, CD_3OD, 25 °C, mix 0.6 s) of TrA. Traces corresponding to: (a) H_1; (b) H_{11}; (c) H_{12ax}; (d) H_{14}; (e) H_4; (f) H_8; (g) H_{21a}; (h) H_{21b}.

3.2.2. HPβCD

A detailed discussion of NMR features of HPβCD is reported in Appendix A Figs. A.2–A.4, Table A.1. The substitution degree, the random nature of the cyclodextrin derivatization as well as the preferential orientation of the hydroxypropyl pendants was demonstrated, which led to an "extended-cavity type" structural arrangement of the cyclodextrin in which the 2-hydroxypropyl chains were directed outwards from the cavity, thus creating an extension of the original truncated cone structure of the cyclodextrin.

3.2.3. TrA/HPβCD complex

The nature of the interaction between TrA and HPβCD, which are responsible for the processes of drug solubilization, was ascertained on the basis of the intermolecular ROEs which were detected in the 2D ROESY spectra. Some difficulties were caused by the very high HPβCD to TrA molar ratio, which was needed in order to obtain detectable solubilized TrA. The most valuable information were obtained by analysing the 2D ROESY traces in the chemical shifts range between 3.62 ppm and 3.91 ppm, in order to cross the spectral regions corresponding to the different types of clusters of resonances of glucosidic units (Fig. 5). Inside the low-frequencies shifted range between 3.62 ppm and 3.76 ppm, ROEs with the H_2 and H_4 protons adjacent to the carbonyl group of the ring A of TrA were observed, with maximum intensities effects due to the H_5 cluster at 3.72 ppm, corresponding to the internal protons adjacent to the smaller diameter inner cavity.

Moving towards the higher frequencies shifted traces which are due to the cluster of protons H_3 on the large part of the internal cavity of the cyclodextrin, the above said ROEs tend to vanish, while an increase of the ROEs with the methyl protons Me-18 and the adjacent olefinic proton H_1 of TrA were observed (Fig. 5).

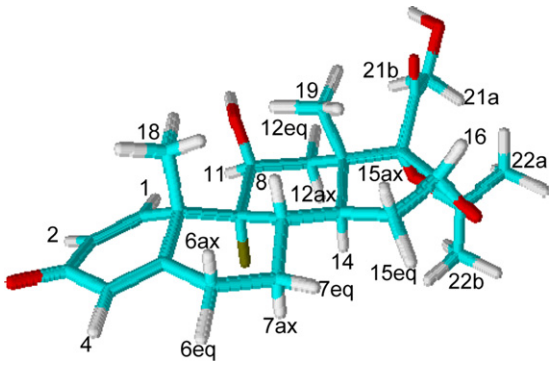

Fig. 4. Graphical representation of the conformation of TrA in solution.

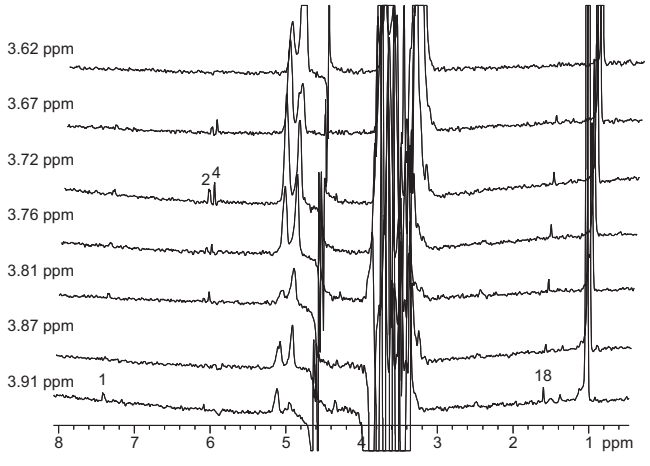

Fig. 5. 2D ROESY (600 MHz, D_2O, 25 °C, mix 0.3 s) of TrA/HPβCD 1:2 mol/mol. Traces corresponding to cyclodextrin protons.

On these bases we conclude that the portion of the TrA molecule which is more extensively involved in the interaction with the cyclodextrin is the ring A, with the carbonyl group pointing at the small sized internal part of the cyclodextrin and the methyl Me-18 directed towards its larger part. The presence of significant populations of TrA/HPβCD adducts with different stereochemistry was not supported by NMR data.

3.3. Preparation of TrA/HPβCD powders

Once established that solubilization process of TrA is accounted for complexation and clarified the nature of interactions between TrA and HPβCD occurring in aqueous solution, we tried to understand if TrA/HPβCD interactions can occur also in the solid state. In fact, the properties of drug/cyclodextrin solid systems are strongly affected by preparation conditions and represent a key factor in determining drug biopharmaceutical features in term of dissolution rate and, as a consequence, of absorption extent through biological barriers. Thus, on the basis of TrA solubility in different aqueous solutions (Appendix A, Table A.2 and Fig. A.5), TrA/HPβCD powders (EP) were produced by drying a TrA water/ethanol/HPβCD solution allowing complete TrA solubilization and thus below 1:3.5 mol ratio (Appendix A, Fig. A.5). Two TrA/HPβCD solids at 1:7 and 1:3.5 molar ratio, named $EP_{1:7}$ and $EP_{1:3.5}$, respectively were obtained and their properties studied in the solid state by Raman spectroscopy, again rationalizing drug/cyclodextrin interactions.

3.4. TrA/HPβCD interaction in the solid state as evaluated by Raman spectroscopy

3.4.1. Interpreting the Raman spectra of TrA and HPβCD

The Raman spectrum of TrA (Fig. 6) displays some 80 peaks in the region from 3200 to 100 cm^{-1}, which makes its complete assignment a rather complex task. To our knowledge, no theoretical analysis of the Raman/IR spectra of the present molecule is available yet; therefore a quantum chemistry investigation was undertaken to deepen the interpretation of the observed Raman peaks in terms of their relative normal modes. The full assignment of the Raman spectrum of TrA is beyond the scope of the present contribution and will be discussed in detail in a forthcoming paper. In the actual context we will focus the attention on the 1750–1550 cm^{-1} region where several intense peaks with no interference from HPβCD signals, are observed.

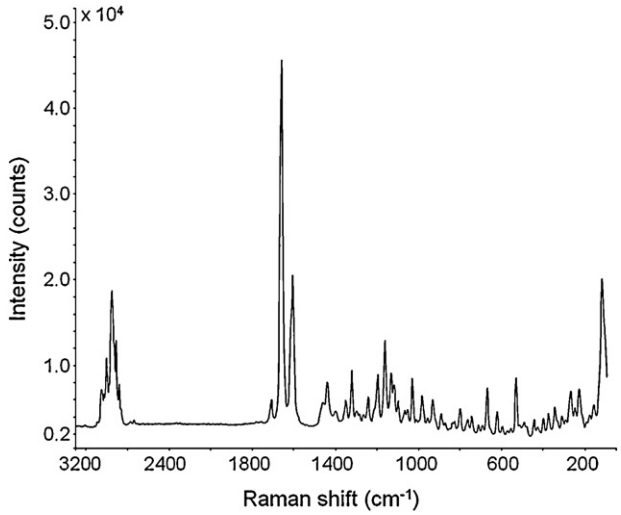

Fig. 6. Raman spectrum of TrA in the 3200–200 cm^{-1} wavenumber range.

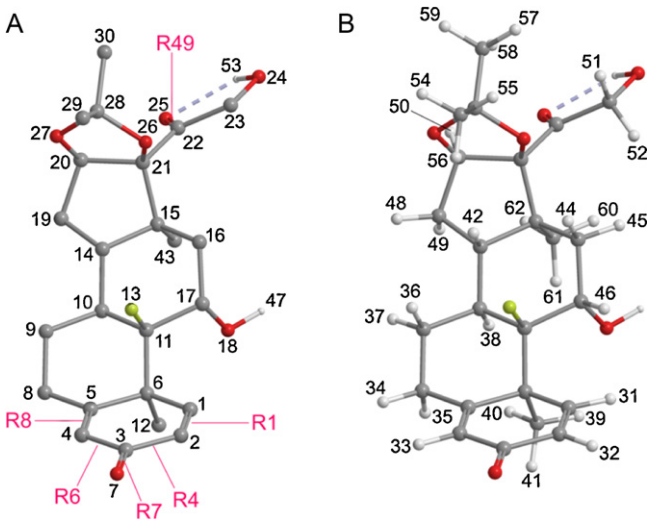

Fig. 7. Geometry of the TrA molecule optimized by the B3LYP/6-31G(d,p) model chemistry. The atom numbering scheme for geometry optimization and normal coordinate analysis is reported (non H-atoms and polar H-atoms in (A); H-atoms in (B). In (A) are also indicated the internal coordinates (bond stretching) contributing to the potential energy distribution of the normal modes reported in Table 1. Atom colour codes are as follows: white = hydrogen; grey = carbon; red = oxygen; yellow = fluorine. (For interpretation of the references to colour in this figure legend, the reader is referred to the web version of the article.)

In a recent study by X-ray diffraction and thermal analysis (Näñther & Jeß, 2006) two distinct polymorphic modifications (Forms I and II) of TrA were identified, whose crystallographic structures were resolved and reported. Form I is a hydrate and is normally used in manufacturing pharmaceutical dosage forms. The small amount of water it contains (1.7 wt%) is responsible for its stability. Form II occurs upon removal of water from Form I or by crystallizing TrA from ethanol.

For the quantum chemistry optimization of the molecular geometry the chosen starting-point was the crystallographic structure denoted as Form II. This is because the theoretical model does not account for molecular interactions with water. In any case, the crystallographic geometry parameters of the isolated molecule relative to Form I result to be very close to those of Form II, which makes less critical the choice of the starting point structure among the two forms.

Quantum chemistry calculations were performed by the DFT method, using the B3LYP hybrid functional and the 6-31G(d,p) basis set. This model chemistry was selected in view of its reliability in predicting the geometry and vibrational behaviour of up to medium sized systems and because it represents, for the problem at hand, the best compromise between predictive accuracy and computational cost.

The optimized geometry of the TrA molecule, represented in Fig. 7, reproduces accurately the crystallographic structure, with a root-mean-squared error (E_{rms}) of 0.011 Å for bond lengths and 0.70 degrees for bond angles. The TrA molecule belongs to the C_1 group (no symmetry), therefore all the 180 modes of vibration are predicted to be IR and Raman active. All the 180 calculated frequencies are positive; the absence of any imaginary frequency confirms that the identified stationary point is a true minimum on the potential energy surface instead of being a saddle point, a necessary condition for the subsequent normal coordinate analysis. By inspection of Fig. 7, it is seen that the O24–H53 group can also form a H-bonding interaction with the ether oxygen O26, which prompted us to explore more closely the potential energy surface searching for possible local minima which may be energetically accessible,

Table 1
Comparison between the spectroscopic parameters calculated by the DFT method (frequency, relative intensity and P.E.D.) and those experimentally observed.

ν_{obs} (cm^{-1})	ν_{calc} (cm^{-1})	Error (%)	I/I_{max} (obs)	I/I_{max} (calc)	P.E.D.[a] (%)
1612	1614	0.1	0.07	0.06	42 R_1 + 38 R_8
1628	1648	1.0	0.05	0.16	29 R_1 + 23 R_7 + 34 R_8
1670	1692	1.2	1	1	67 R_7 + 7 R_1 + 5 R_4 + 5 R_6 + 6 R_8
1716	1707	0.6	0.07	0.10	89 R_{49}

[a] Contributions lower than 5% were neglected.

and hence relevant for isolated molecules *in vacuo* or in an inert solvent, as opposed to the crystal cell environment.

To reduce computational cost, the problem was tackled by using the Molecular Mechanics (MM) approach. In particular, the MM2 force field was selected because, in its more advanced formulation, it can account for H-bonding. In fact, MM2 does not contain an explicit H-bonding term, but handles the interaction through the van der Waals potential by reducing the vdW radius of the hydrogen involved and by increasing the vdW constant by 1–3 kcal/mol, depending on the molecular environment. It has been demonstrated that in such a way it is possible to satisfactorily reproduce *ab initio* calculations on compounds in which a hydroxyl hydrogen is H-bonded to another hydroxyl, an amide or a carbonyl group (Allinger et al., 1988).

The potential energy scan, performed by changing stepwise (5° increment) the torsion angle θ(O25–C22–C23–O24), (Appendix A, Fig. A.7) demonstrates that the structure represented in Fig. 7 and A.7 (Appendix A) corresponds to a pronounced minimum, while the formation of a H-bonding interaction between the O24—H53 hydroxyl and the O26 ether oxygen generates a significantly less stable local minimum ($\Delta E \cong 9$ kcal/mol), which, according to the Boltzmann distribution law, is not appreciably populated. This result further justifies the use of structure A as global minimum for normal coordinates analysis.

Towards a comparison between the calculated and observed Raman spectra, we first note that the experimental spectrum of TrA in the crystalline state does not represent an appropriate reference. In fact, the theoretical description of the molecule (considered as isolated *in vacuo*) does not account for the strong crystal-field effects occurring within the crystalline structure. A more meaningful experimental reference is represented by a diluted solution in an essentially inert, low polarity solvent. In this environment, owing to the absence of strong, site-specific molecular interactions, the solvent can be treated as a continuous medium and, because of the dilution, no self-association among TrA molecules is likely to occur. Thus, Fig. 8A displays a comparison between the Raman spectrum collected on a saturated solution of TrA in chloroform (concentration lower than 1.0 wt%) and the spectrum calculated theoretically. The experimental profile is reported along with its curve-resolved components as obtained by LSCF analysis. Qualitatively, the theoretically computed spectrum (Fig. 8A, trace b) correctly predicts the occurrence, in the frequency range of interest, of four components, with one of the peaks being about one order of magnitude more intense than the other three, which display comparable intensities. A more quantitative analysis (see Table 1) reveals a very satisfactory agreement between the calculated and observed peak positions (minimum error 0.1%, maximum 1.2%, $E_{rms} = 15.2\ cm^{-1}$). Also the relative intensities of the different components are reproduced remarkably well by the calculation, with the partial exception of the mode at 1628 cm^{-1}, whose relative intensity is theoretically overestimated by a factor of 3. On the whole, the agreement between calculated and observed parameters is well within the performance limits of the computational method employed (Sousa, Fernandes, & Ramos, 2007) and, therefore, the description of the normal modes giving rise to the investigated Raman peaks, is to be considered highly reliable.

By inspection of the form of the normal modes (Appendix A, Fig. A.8) and of the relative animated motions, and taking into consideration the relative PED's, the vibrations giving rise to the observed peaks can be described as follows:

- Peak at 1612 cm^{-1}: an out-of-phase stretching of the two C=C bonds of the C1—C2—C3—C4—C5—C6 ring.
- Peak at 1628 cm^{-1}: this vibration involves simultaneously the stretching of the two C=C bonds and of the carbonyl bond in the same ring structure. The two C=C bonds vibrate in phase with each other and out-of-phase with the carbonyl. The mechanical coupling among the stretching modes produces a slight contribution of the C1—C6—C5 bending.
- Peak at 1669 cm^{-1}: The C3—O7 carbonyl stretching contributes most to this mode. The stretching of the two C=C bonds of the ring is also involved but to a very limited extent. The three bonds vibrate in phase. Also in this case the mechanical coupling produces a contribution of the C2—C3—C4 bending which is evident in terms of atomic displacements but negligible in terms of PED because of the reduced value of the bending force constant with respect to the other force constants involved.
- Peak at 1716 cm^{-1}: the essentially isolated vibration of the C22—O25 carbonyl.

The Raman spectrum of HPβCD is described in depth in Appendix A (comment to Fig. A.6). Having unambiguously identified the vibrational origin of the TrA peaks in the unperturbed, reference state, it is now possible to proceed with the interpretation of the features observed in the spectra of the crystalline TrA and the TrA/HPβCD $EP_{1:7}$.

Fig. 8B compares the Raman spectra, in the 1550–1790 cm^{-1} range, of crystalline TrA (trace a), TrA solubilized in chloroform (trace b) and the $EP_{1:7}$ (trace c). The latter spectrum is reported together with the curve-resolved components as obtained by applying the LSCF method (see Section 2). The results of the curve-fitting analysis of the three experimental profiles are summarized in Appendix A, Table A.3. Obvious differences are apparent between spectra a and b. The crystalline spectrum displays the splitting of the main peak in two components, centred, respectively, at 1663 and 1670 cm^{-1}. The position of the high frequency component is essentially coincident with that of the main peak in the solution spectrum, which is an evidence against a crystal-field splitting. The latter, in fact, would preferentially produce a doublet equally spaced with respect to the unperturbed reference line. Also, for a crystal-field effect, the intensities of the doublet components are generally comparable. A more reasonable interpretation of the splitting relies on the occurrence, within the crystalline arrangement of the molecules, of an inter-molecular H-bonding interaction between the C3—O7 carbonyl (responsible for the 1670 cm^{-1} peak) and one of the TrA hydroxyls. This, as is generally the case, produces a lowering of the C=O force constant, and a red-shift of the relative peak. Only a fraction of the C3—O7 carbonyls are involved, as indicated by the two component structure of the crystalline spectrum in the 1640–1700 cm^{-1} interval. The occurrence of the intermolecular interaction just described is confirmed by the crystallographic data (Näñther & Jeß, 2006).

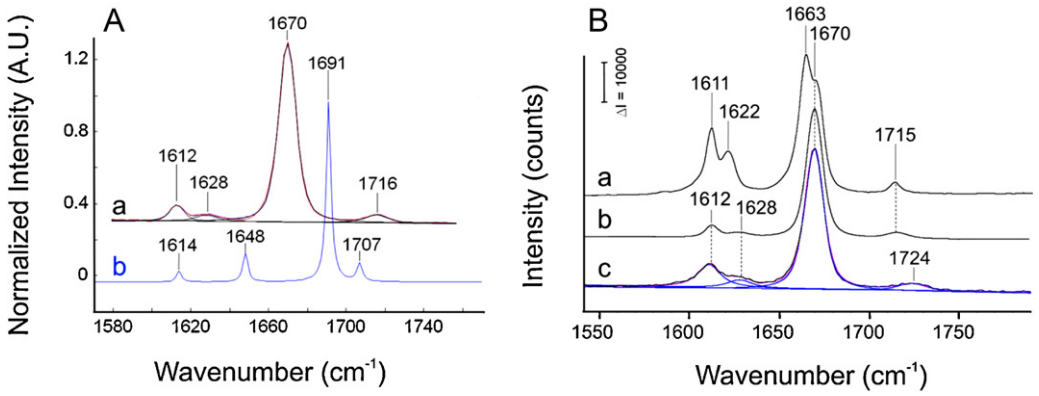

Fig. 8. (A) Comparison between the experimental Raman spectrum of TrA in a saturated chloroform solution (trace a) and the Raman spectrum calculated theoretically with the DFT method (trace b). The spectra have been normalized with respect to the peak of highest intensity and have been arbitrarily displaced along the *Y* axis to facilitate the comparison. The experimental spectrum is displayed along with its curve-resolved components as obtained by LSCF analysis. (B) Raman spectrum in the 1540–1790 cm^{-1} range of crystalline TrA (trace a); chloroform solution (trace b); TrA/HPβCD EP (trace c; molar ratio TrA/HPβCD = 1:7). The spectrum of EP is reported together with its curve-resolved components as obtained by LSCF analysis.

These results evidence the sensitivity of the carbonyl peaks towards the detection of H-bonding with hydroxyl groups acting as proton donors. Furthermore, the specificity of the TrA spectrum in the 1550–1770 cm^{-1} range makes it a sensitive and diagnostic signature to identify the presence of a crystalline structure. More on this later.

The spectrum of TrA/HPβCD $EP_{1:7}$ closely resembles that of the chloroform solution (compare Fig. 8B, traces b and c and the data in Table A.3). In particular, the components at 1611, 1628 and 1669 cm^{-1} display coincident parameters (within experimental uncertainty) in terms of position, band-shape and FWHH. The peak at the highest frequency is the sole showing significant differences with respect to the reference: its position shifts toward higher wavenumbers by 8 cm^{-1} and its FWHH increases by 4 cm^{-1}. The peaks coincident in the EP and in the chloroform solution are those of the C1—C2—C3—C4—C5—C6 ring (double bonds and the carbonyl group), which suggests that in the EP the C1—C2—C3—C4—C5—C6 ring remains unperturbed with respect to the reference state. On the contrary, the significant changes observed for the C22—O25 carbonyl peak are supportive of the involvement of such functional group in an interaction with HPβCD.

The above results indicate that no self-association of TrA takes place within TrA/HPβCD $EP_{1:7}$. In fact, this association would necessarily involve intermolecular H-bonding at the carbonyl groups, which are very sensitive to these interactions and, as in the case of the crystalline spectrum, would show clear evidence of a two component band-shape and/or a detectable red-shift. We conclude, therefore, that in TrA/HPβCD $EP_{1:7}$. TrA is molecularly dispersed in the HPβCD matrix. The observed displacement of the C22—O25 carbonyl peak at higher wavenumbers implies a strengthening of the C=O force constant, which is what one would expect upon the breaking of an H-bond. Thus, one possibility is that the interaction of TrA with HPβCD sampled by Raman spectroscopy occurs through the O24—H53 hydroxyl group with the external hydrophilic surface of cyclodextrin. This, in turn, causes the dissociation of the O24—H53/C22—O25 intramolecular interaction, resulting in the isolation of the carbonyl group.

The considerable peak broadening observed in the case of the $EP_{1:7}$ with respect to the chloroform solution and, even more so, to the crystalline spectrum has been related to a decrease of the vibrational relaxation time of the specific functional group, generally associated with a weaker interaction with the molecular environment (Iliescu, Baia, & Miclaus, 2004; Turner, 2002). This interpretation is in line with the hypothesis of a carbonyl group no longer involved in H-bonding.

The observation that the peaks originating from the C1—C2—C3—C4—C5—C6 ring in the EP retain the same spectral parameters as those in the reference state points to a close molecular environment in the two cases, *i.e.* a hydrophobic medium with no site-specific interactions. In the EP this environment is more likely to correspond to the cavity interior rather than to the external hydrophilic surface rich of hydroxyl groups with a high propensity to interact with the carbonyls. Along the same line of reasoning, Lamcharfi, Kunesch, Meyer, and Robert (1995), in a vibrational spectroscopy investigation on several inclusion complexes, obtained analogous results and concluded that "inclusion acts like an isolation of the guest molecules from encounters and leads to a narrowing of the lines analogous to solvent effects".

In summary, the evidence provided by Raman spectroscopy is compatible with the picture emerging from the NMR analysis which indicates that the C1—C2—C3—C4—C5—C6 ring (ring A) is included in the cavity, while the hydroxyacyl chain interacts preferentially with polar sites located outside the cavity.

3.4.2. *Raman imaging of TrA/HPβCD solid systems*

Confocal Raman spectroscopy is highly effective for investigating potentially heterogeneous systems in the solid-state and hence for revealing the distribution of TrA in HPβCD, making use of the spectroscopic contrast among the mixture components. In particular, the absence of inelastic scattering in the wavenumber region 1550–1800 cm^{-1} for HPβCD allows the detection of interference-free signals from TrA even when its content is relatively low.

The Raman image collected on a 13 μm × 13 μm surface of a TrA/HPβCD $EP_{1:7}$ is shown in Fig. 9A. The image has been obtained considering the intensity ratio between the TrA peak at 1670 cm^{-1} and the HPβCD peak at 1457 cm^{-1}. This spectroscopic parameter is proportional to the TrA/HPβCD molar ratio in the mixture. The uniform colour pattern of Fig. 9A (which corresponds to a I_{1670}/I_{1457} ratio of 4.5 ± 0.3 on the colour-map scale) indicates a constant TrA/HPβCD molar ratio throughout the sample, which, in turn, suggest the formation of a TrA/HPβCD complex when the components are mixed in the present composition. When the amount of TrA is increased to reach a molar ratio 1:3.5 ($EP_{1:3.5}$), different features are observed in the Raman image. In the sampled area a TrA domain having a size of about 15 μm × 10 μm is detected. The Raman spectrum of this feature (see inset a of Fig. 9B) is characteristic of the TrA crystalline phase and no HPβCD peaks are present. Evidently, in this sample, the TrA concentration is above the solubility threshold, which causes the TrA precipitation to occur. Aside the crystal

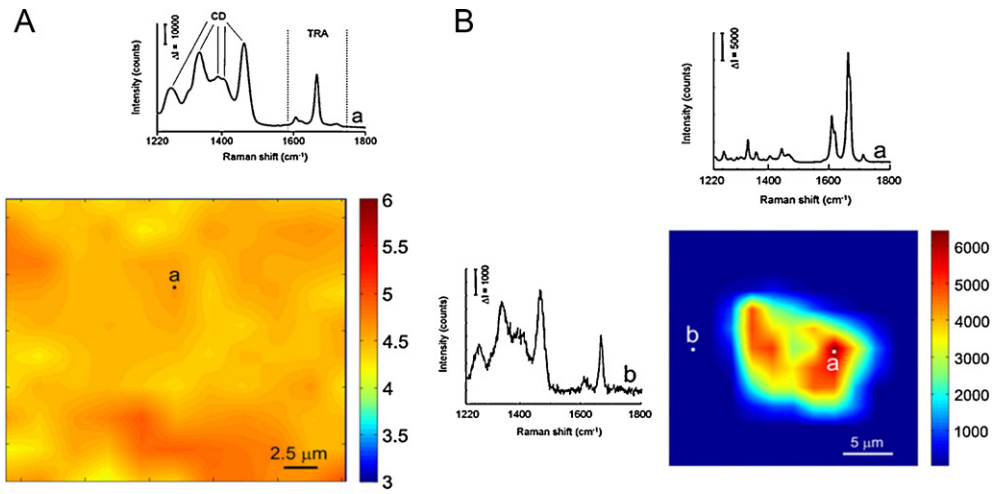

Fig. 9. Raman image of the TrA/HPβCD EP. (A) TrA/HPβCD EP with molar ratio 1:7. The inset display the spectrum collected at the indicated position. Image obtained by considering the intensity ratio I_{1670}/I_{1457}. (B) TrA/HPβCD EP with molar ratio 1:3.5. The insets display the spectra collected at the indicated positions. The Raman image has been obtained by considering the intensity of the TrA peak at1670 cm^{-1}.

(*i.e.* in the blue region of Fig. 9B), the spectrum displays the signals of both TrA and HPβCD (see inset b), and the ratio I_{1670}/I_{1457} is constant and close to the value observed for the 1:7 composition (4.0 ± 0.5). This behaviour is again consistent with a system having reached saturation.

4. Conclusion

We demonstrate here that the combined use of several solution and solid state spectroscopic techniques allows to shed light on the molecular basis of the solubilization processes of highly lipophilic TrA in its formulations containing HPβCD as solubilization agent. The main contribution of the combined use of NMR and Raman techniques can be focused on the opportunity they offer to gather together several stereochemical details regarding the drug, the cyclodextrin and the drug–cyclodextrin complex both in the solution and solid states.

In the evaluation of the association constant by solubility measurements, the relevance of the intrinsic solubility of the drug was confirmed, which affects critically the value of the association constant, where the 1:1 drug to cyclodextrin complexation stoichiometry is assumed.

In aqueous solvents and hydrogen bond donor solvents, which better mimic the aqueous environment, the rigid structure of TrA shows small tendency to self-aggregate, but, in any case, the hydroxyacyl moiety is engaged in an intramolecular hydrogen bond interaction with the adjacent carbonyl group. In the aqueous medium, HPβCD does not perturb the conformation of TrA, as only its ring A is inserted into the cavity of the cyclodextrin from its large rim, with the carbonyl group of A pointing at the inner narrower part of the cavity of the host. In this way, the hydrophilic portion of TrA remains exposed to water and to hydrophilic pendants of the cyclodextrin. This mechanism of interaction is reasonably favoured by the expanded structure of the cyclodextrin due to the presence of the hydroxypropyl chains which are exposed to the aqueous medium. The NMR results do not exclude the possible coexistence of different interaction mechanisms, which could involve the outer surface of the cyclodextrin and the hydroxyacyl chain of TrA, as detected by the Raman technique. These mechanisms of interaction, which seems to play a relevant role in the solid state, are less favoured in aqueous medium or, alternatively, they do not generate constraints of spatial proximity suitable for ROEs observations. Raman imaging experiments in the solid state confirmed the attainment of a molecularly homogeneous system when the TrA/HPβCD molar ratio is 1:7. However, for mixtures richer in TrA (1:3.5) the latter crystallizes forming domains whose size is in the range of 10–15 μm. This aspect should be taken into account when preparing fast-dissolving binary systems of TrA with HPβCD.

As a final remark, it must be stressed that such a kind of differentiated information could not have been gained without the combined use of several spectroscopical and computational techniques, with differentiated responsiveness. The approach proposed can be beneficial in preformulation studies providing the necessary ground-work for formulation development on the bases of a rational design.

Acknowledgements

The work was supported by MIUR (Project "Design, synthesis and study of innovative molecules and materials with enhanced molecular recognition properties: applications to high performance chromatographic separation systems" grant 2009ZSC5K2) and ICCOM-CNR.

Appendix A. Supplementary data

Supplementary data associated with this article can be found, in the online version, at http://dx.doi.org/10.1016/j.carbpol.2012.06.075.

References

Allinger, N. L., Kok, R. A., & Imam, M. R. (1988). Hydrogen bonding in MM2. *Journal of Computational Chemistry*, *9*, 591–595.
Becke, A. (1993). Density-functional thermochemistry. III. The role of exact exchange. *The Journal of Chemical Physics*, *98*, 5648–5652.
Brewster, M. E., & Loftsson, T. (2007). Cyclodextrins as pharmaceutical solubilizers. *Advanced Drug Delivery Reviews*, *59*, 645–666.
Duchêne, D. (2011). Cyclodextrins and their inclusion complexes. In *Cyclodextrins in pharmaceutics, cosmetics and biomedicine*. John Wiley & Sons, Inc., pp. 1–18
Foster, R., & Fyfe, C. A. (1965). Interaction of electron acceptors with bases. Part 15.-Determination of association constants of organic charge-transfer complexes by n.m.r. spectroscopy. *Transactions of the Faraday Society*, *61*, 1626–1631.
Frisch, M. J., Trucks, G. W., Schlegel, H. B., Scuseria, G. E., Robb, M. A., Cheeseman, J. R. et al. (2004). Gaussian 03, Revision C.02 Gaussian, Inc., Wallingford CT [Computer software].
Hendra, P. J. (2006). Sampling considerations for Raman spectroscopy. In *Handbook of vibrational spectroscopy*. John Wiley & Sons, Ltd.
Higuchi, T., & Connors, K. A. (1965). Phase solubility techniques. In C. N. Reilley (Ed.), *Advances in analytical chemistry and instrumentation*. New York: Wiley-Interscience, 117–212.

Iliescu, T., Baia, M., & Miclaus, V. (2004). A Raman spectroscopic study of the diclofenac sodium–beta-cyclodextrin interaction. *European Journal of Pharmaceutical Sciences*, *22*, 487–495.

Johnson, C. S. (1999). Diffusion ordered nuclear magnetic resonance spectroscopy: Principles and applications. *Progress in Nuclear Magnetic Resonance Spectroscopy*, *34*, 203–256.

Keresztury, G. (2002). Raman spectroscopy: Theory. In J. M. Chalmers, & P. R. Griffiths (Eds.), *Handbook of vibrational spectroscopy* (pp. 71–87). New York: John Wiley & sons, Ltd.

Keresztury, G., Holly, S., Besenyei, G., Varga, J., Wang, A. Y., & Durig, J. R. (1993). Vibrational-spectra of monothiocarbamates. 2. Ir and Raman-spectra, vibrational assignment, conformational-analysis and ab-initio calculations of S-methyl-N,N-dimethylthiocarbamate. *Spectrochimica Acta Part A-Molecular and Biomolecular Spectroscopy*, *49*, 2007–2026.

Lamcharfi, E., Kunesch, G., Meyer, C., & Robert, B. (1995). Investigation of cyclodextrin inclusion compounds using FT-IR and Raman spectroscopy. *Spectrochimica Acta Part A-Molecular and Biomolecular Spectroscopy*, *51*, 1861–1870.

Loftsson, T., & Duchêne, D. (2007). Cyclodextrins and their pharmaceutical applications. *International Journal of Pharmacy*, *329*, 1–11.

Loftsson, T., Hreinsdottir, D., & Masson, M. (2007). The complexation efficiency. *Journal of Inclusion Phenomena and Macrocyclic Chemistry*, *57*, 545–552.

Loftsson, T., Hreinsdottir, D., & Masson, M. (2005). Evaluation of cyclodextrin solubilization of drugs. *International Journal of Pharmacy*, *302*, 18–28.

Loftsson, T., Magnusdottir, A., Masson, M., & Sigurjonsdottir, J. F. (2002). Self-association and cyclodextrin solubilization of drugs. *Journal of Pharmaceutical Science*, *91*, 2307–2316.

Meier, R. J. (2005). On art and science in curve-fitting vibrational spectra. *Vibrational Spectroscopy*, *39*, 266–269.

Näñther, C., & Jeß, I. (2006). New news about an old drug: Investigations on the polymorphism of triamcinolone acetonide. *Angewandte Chemie International Edition*, *45*, 6381–6383.

Shrader, B. (2002). FT-Raman spectroscopy. In J. M. Chalmers, & P. R. Griffiths (Eds.), *Handbook of vibrational spectroscopy* (pp. 1289–1301). New York: John Wiley & sons, Ltd.

Smith, E., & Dent, G. (2005). *Modern Raman spectroscopy: A practical approach*. Chichester: John Wiley & Sons, Ltd.

Sousa, S. F., Fernandes, P. A., & Ramos, M. J. (2007). General performance of density functionals. *Journal of Physical Chemistry A*, *111*, 10439–10452.

Turner, J. J. (2002). Bandwidths. In J. M. Chalmers, & P. R. Griffiths (Eds.), *Handbook of vibrational spectroscopy* (pp. 101–127). New York: John Wiley & Sons, Ltd.

Waring, M. J. (2010). Lipophilicity in drug discovery. *Expert Opinion on Drug Discovery*, *5*, 235–248.

Wilson, E. B., Decius, J. C., & Cross, P. C. (1955). *Molecular vibrations*. New York: McGraw-Hill.

Wimmer, R., Aachmann, F. L., Larsen, K. L., & Petersen, S. B. (2002). NMR diffusion as a novel tool for measuring the association constant between cyclodextrin and guest molecules. *Carbohydrate Research*, *337*, 841–849.

Wong, M. W., Wiberg, K. B., & Frisch, M. (1991). Hartree-Fock 2nd derivatives and electric-field properties in a solvent reaction field – theory and application. *Journal of Chemical Physics*, *95*, 8991–8998.